Journal of the North for Basic and Applied Sciences, Vol. (8), Issue (1), (May 2023/ Shawwal 1444 H) 46-62

KINGDOM OF SAUDI ARABIA
Northern Border University (NBU)
Journal of the North for Basic & Applied Sciences(JNBAS)
p - ISSN : 1658 -7022 / **e-ISSN: 1658 - 7014**
www.nbu.edu.sa
s.journal@nbu.edu.sa

Self-cleaning Construction Material for Water Depollution Using Photo-catalytic Degrdation of Crystal Violet by ZnO-nanoparticles Catalyst

Yahya Alassaf

(Received 28/3/2023 ; accepted 31/5/2023)

Abstract: The role of self-cleaning building materials in reducing water pollution besides their durability has attracted a lot of consideration. The inclusion of this material is now more important than ever due to the dramatic increase in domestic and industrial pollution sources that degrade water quality. The application of photo-catalytic self-cleaning concrete to remove organic impurities from water is the major consideration of this work. Using a response surface methodology (RSM), the experimental design for nanoparticle synthesis was optimized. The effect of stirring speed, the temperature and the concentration of zinc acetate on the nanoparticles diameter were studied. A Box-Behnken (BB) design with three factors and three center points was used. The size of the synthesized particles is most significantly influenced by temperature. The degradation results of the pollutant model (Crystal Violet (CV)) are carried out for different sizes of synthesized particles (14.2 nm, 16.8 nm, 19 nm) and an average particle size of commercial ZnO (50 nm). The results show that decreasing the particle size from 50 nm to 14.2 nm improves the maximum conversion rate by 33% and accelerates the reaction rate by 28%. The concentration of pollutant decreases gradually to reach the values of 4.30 mg/L, 1.80 mg/L, and 0.85 mg/L for the respective times 5min, 10min and 23min. The maximum conversion rate achieved is 91.5%. Finally, to validate the numerical model simulating the self-cleaning concrete paving block, a comparison of the experimental and modeled reaction rates was established. The modeling results accurately matched the experimental results.

Keywords: Self-cleaning, Concrete paving block, Nanoparticles, Photo-catalyst, RSM, Modeling and simulation.

DOI: 10.12816/0061503

* **Corresponding Author:**
Assistant professor, Civil Engineering, College of Engineering, Northern Border University, P.O. Box1321, Code: 91431 City: Arar, Kingdom of Saudi Arabia.
e-mail: yahya.alassaf@nbu.edu.sa

المملكة العربية السعودية
جامعة الحدود الشمالية (NBU)
مجلة الشمال للعلوم الأساسية والتطبيقية (JNBAS)
طباعة ردمد: 1658-7022/ إلكتروني – ردمد: 1658-7014
www.nbu.edu.sa
s.journal@nbu.edu.sa

مواد تشييد ذاتية التنظيف لإزالة تلوث المياه باستخدام التحلل التحفيزي الضوئي للبنفسج الكريستالي بواسطة محفز الجسيمات النانوية ZnO

يحيى صالح العساف

(قدم للنشر في 1444/9/6؛ وقبل للنشر في 1444/11/11هـ)

مستخلص البحث: لقد اجتذب دور مواد البناء ذاتية التنظيف في تقليل تلوث المياه إلى جانب متانتها الكثير من الاهتمام. أصبح إدراج هذه المواد الآن أكثر أهمية من أي وقت مضى بسبب الزيادة الهائلة في مصادر التلوث المنزلية والصناعية التي تقلل من جودة المياه. يعتبر تطبيق الخرسانة ذاتية التنظيف ذات التحفيز الضوئي لإزالة الشوائب العضوية من الماء الاعتبار الرئيسي لهذا العمل. باستخدام منهجية سطح الاستجابة (RSM) ، تم تحسين التصميم التجريبي لتخليق الجسيمات النانوية. تمت دراسة تأثير سرعة التحريك ودرجة الحرارة وتركيز خلات الزنك على قطر الجسيمات النانوية. تم استخدام تصميم Box-Behnken (BB) مع ثلاثة عوامل وثلاث نقاط مركزية. يتأثر حجم الجسيمات المصنعة بدرجة كبيرة بدرجة الحرارة. تم إجراء نتائج تحلل نموذج الملوثات (Crystal Violet (CV)) لأحجام مختلفة من الجسيمات المركبة (14.2 نانومتر ، 16.8 نانومتر ، 19 نانومتر) ومتوسط حجم الجسيمات من ZnO التجاري (50 نانومتر). أظهرت النتائج أن تقليل حجم الجسيمات من 50 نانومتر إلى 14.2 نانومتر يحسن معدل التحويل الأقصى بنسبة 33٪ ويسرع معدل التفاعل بنسبة 28٪. ينخفض تركيز الملوث تدريجياً ليصل إلى قيم 4.30 مجم / لتر و 1.80 مجم / لتر و 0.85 مجم / لتر لكل الأوقات 5 دقائق و 10 دقائق و 23 دقيقة. أقصى معدل تحويل تم تحقيقه هو 91.5٪. أخيرًا ، للتحقق من صحة النموذج العددي الذي يحاكي كتلة الرصف الخرسانية ذاتية التنظيف ، تم إجراء مقارنة بين معدلات التفاعل التجريبية والنمذجة. نتائج النمذجة تتطابق بدقة مع النتائج التجريبية.

كلمات مفتاحية: التنظيف الذاتي، كتلة الرصف الخرسانية، الجسيمات النانوية، المحفز الضوئي، منهجية سطح الاستجابة، النمذجة والمحاكاة.

للمراسلة:
أستاذ مساعد، الهندسة المدنية، كلية الهندسة، جامعة الحدود الشمالية. ص ب: 1321 رمز بريدي: 91431. عرعر, المملكة العربية السعودية

e-mail: yahya.alassaf@nbu.edu.sa

DOI: 10.12816/0061503

1. INTRODUCTION

Self-cleaning construction materials have attracted exceptional attention for their inescapable role in water and air pollution control and their durability (Awadalla, Zain, Kadhum, & Abdalla, 2011; Paolini, Borroni, Pedeferri, & Diamanti, 2018; Qualharini, Stolz, Martini, Polesello, & da Silva, 2023; Xia et al., 2023). The integration of this type of material has become more urgent with the huge increase in the sources of domestic and industrial pollution affecting air and water quality (Deng, 2021; Karpińska & Kotowska, 2019; Singh, Yadav, Kathi, & Singh, 2022). In order to eliminate any residual pollution from surface water, it is necessary to apply advanced oxidation techniques (AOT) which can be envisaged for the destruction of traces of residual pollution (Lee & Park, 2013; Pattnaik, Sahu, Poonia, & Ghosh, 2023; Yao et al., 2023). Among these techniques we can cite: Ozonation, the use of UV rays and photo-catalysis. Zinc oxide nanoparticles, is considered one of the most important photo-catalyst for organic pollutant degradation (Mishra, Pandey, & Fosso-Kankeu, 2023; Wouters et al., 2023). In the other hand, the water scarcity in Saudi Arabia is one of the most important contemporary problems and is of great interest at the research level. The strategic studies of the Ministry of Environment, Water and Agriculture in KSA showed the urgent need to rationalize the demand for water, which was estimated at more than 25 billion cubic meters with an annual increase of 8% (Alrwis et al., 2021; Baig, Alotibi, Straquadine, & Alataway, 2020). It is in this approach that the national and international demand for the development of adequate water treatment techniques and the use of self-cleaning material has become a major preoccupation (Hassan, Yilbas, Al-Sharafi, Sahin, & Al-Qahtani, 2020; Wu et al., 2021). Many of discovered pollutants, especially persistent organic pollutants POPs, are not degradable by conventional water treatment methods. Consequently, it is necessary to apply advanced oxidation (AOT) such as photo-catalysis. Advanced oxidation process (AOP) relies on the production of highly reactive oxidative species, particularly OH° radicals, in particular because of its non-selectivity (Gaur, Dutta, Singh, Dubey, & Kamboj, 2022; Iqbal, Yusaf, Usman, Hussain Bokhari, & Mansha, 2023). Advanced treatment of water is mainly based on photo-catalysis which encompasses a variety of reactions including decomposition processes of chemical species (Caudillo-Flores, Muñoz-Batista, Fernández-García, & Kubacka, 2022; V. Singh et al., 2022). When it is exposed to UV radiation, the photons are absorbed and an electron migrates to the conduction band leaving a hole in the valence band (Van Thuan et al., 2022). Modern photo-catalytic applications involve doping with fluorescent nanoparticles. It promotes the reduction of the electron-hole recombination phenomenon and enhance catalytic efficiency. The significant specific surface area (surface to volume ratio) of nanomaterials improves the adsorption of contaminants and the degradation of pollutants (Napoli, Uriarte, Garrido, Domini, & Acebal, 2022; Ningthoujam et al., 2022; Song et al., 2022). ZnO is frequently applied to reduce water pollution through advanced oxidation processes and is widely employed as a semi-conductor photo-catalyst (Abukhadra, AlHammadi, Khim, Ajarem, & Allam, 2022; Modi et al., 2022). The majority of nanoparticles qualities are closely correlated with its size and shape. By using a series of hydrolysis-condensation reactions, metal alkoxides, which are primarily composed of a metal atom encircled by simple alkyl groups, are converted into nanoparticles. Due to a phenomenon known as "quantum confinement," the major property of semiconductor nanocrystals is that their band gap can be altered in accordance with their size (Ahamed, Ahamed, Kumar, & Sivaranjani, 2022; Torres-Torres & García-Beltrán, 2022). The gap widens and the energy levels are constrained to discrete values as a result of the charge carriers' need to take more kinetic energy in order to penetrate the nanocrystal. The energy structure transitions from a band structure to a discrete level structure as a result of the nanometric size of the nanocrystals (El-Morsy, Awwad, Ali, & Menazea, 2022; Kalyani & Dhoble, 2023). Thus, the properties of the nanoparticles are intermediate between those of the bulk material and those of the molecular compounds, and the theory of the

molecular orbitals is more suited to describe them than the valence band (BV) and conduction band (BC) of solid semiconductors (Gul et al., 2022; Lvov, Potemkin, & Stremoukhov, 2023).
The main problem in this research concerns the remove of organic pollutants from water using photo-catalytic self-cleaning concrete. The enhancement of the catalyst for photo-catalytic degradation, like natural ZnO, is based on the use of nanoparticles in order to stabilize the catalyst and to avoid electron-hole recombination phenomena in the semiconductor. In this work, an addition of catalyst (ZnO) doped by nanoparticles on the concrete was carried out. The synthesis of nanoparticles passes through several preparation stages such as dissolution, centrifugation and extraction of nanoparticles based on ZnO. Then, concrete blocks are prepared by introducing the synthesized photo-catalyst on its surface. A series of photo-catalytic tests are carried out choosing Crystal Violet (CV) as the typical pollutant. Finally, a modeling of the catalytic degradation is performed using the finite element method.

2. MATERIAL AND METHODS

The preparation of self-cleaning concrete paving block takes place in several stages. The first stage consists of synthesizing the activated nanoparticles. The structure and crystallinity of the prepared nano-powders were analyzed by X-Ray Diffraction (XRD) utilizing D8 Advance Bruker diffractometer (Liu, Liu, Yu, Copeland, & Wang, 2023). The catalyst thus prepared will be deposited on the surface of the concrete paving block. To test the self-cleaning efficiency of the concrete, several photo-catalytic tests were performed.

2.1 Preparation of ZnO nanoparticles

ZnO nanoparticles were prepared using the sol-gel method. Zinc acetate dehydrate Zn-$(CH_3COO)_2,2H_2O$, was dissolved in a mixture of deionized water/ethanol and by adding NaOH under agitation.
Then the solution obtained is placed under centrifugation at 3000 rpm for 5 min and the supernatant is then filtered to recover the particles in suspension in addition to those already decanted by centrifugation. Finally, the synthesized nanoparticles are dried and calcined at 500°C.On the other hand, a response surface methodology was used to optimize the experimental conduct of nanoparticle synthesis. The effect of stirring speed, the temperature and the concentration of zinc acetate on the nanoparticles diameter were studied. The nanoparticle synthesis steps are described in the figure1:

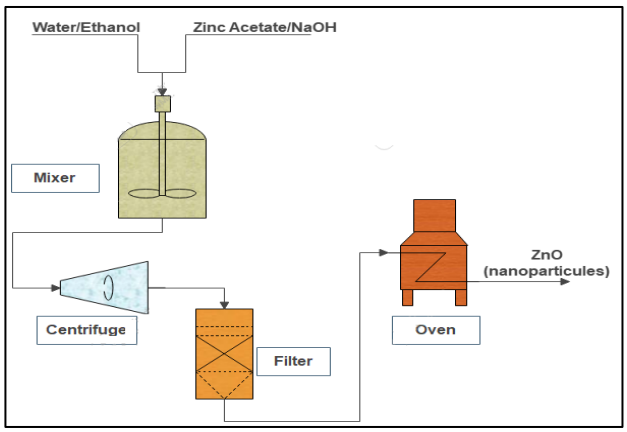

Figure 1: ZnO nanoparticle synthesis steps.

The tables 1 groups the experimental conditions for the synthesis of ZnO nanoparticles. A Box-Behnken (BB) design with three factors and three center points was used.

Table1: Design Summary- Box-Behnken (BB) Design.

Box-Behnken (BB) design: 3 factors and 3 center points				
Experimental design				**Graphical representation**
Factors	3	Replicates	1	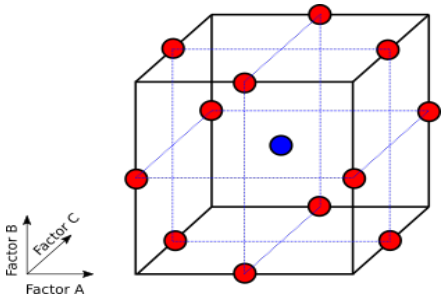
Base runs	15	Total runs	15	
Base blocks	1	Total blocks	1	

In this design the factors studied (concentration of zinc acetate, temperature, and stirring speed) are considered as continuous variables and are grouped in table 2:

Table 2: ZnO nanoparticles synthesis factor design.

StdOrder	RunOrder	[Zn-(CH3COO)2,2H2O] (mmol/L)	Temperature (°C)	Stirring time (hr)
13	1	0.25	65	3.5
7	2	0.10	65	5.0
11	3	0.25	50	5.0
9	4	0.25	50	2.0
6	5	0.40	65	2.0
8	6	0.40	65	5.0
2	7	0.40	50	3.5
5	8	0.10	65	2.0
10	9	0.25	80	2.0
1	10	0.10	50	3.5
15	11	0.25	65	3.5
12	12	0.25	80	5.0
3	13	0.10	80	3.5
4	14	0.40	80	3.5
14	15	0.25	65	3.5

2.2 Characterizations of ZnO NPs

The produced nanoparticles structure and crystallinity were examined using X-ray diffraction (XRD) on a D8 Advance Bruker diffractometer with Cu-K radiation (λ = 0.15406 nm) at an accelerating voltage of 40 kV in the 20–80° range. Using Scherer's equation (1), the mean crystallite size (dp) value has been calculated (Hossain, Jahan, & Ahmed, 2023).

$$dp = \frac{K\,\lambda}{\beta\,cos\theta} \quad (1)$$

Where λ is the wavelength (λ = 0.154056 nm), β is the full width at a half-maximum (FWHM) (ie.

Broadening of the peak), θ is the corresponding diffraction angle, and K the shape constant.

2.3 Photo-catalytic activity tests

The photo-catalytic degradation of the pollutant - Crystal Violet (CV)-, is carried out on the surface of the concrete paving block. The concrete paving block is placed in the reactor containing an initial concentration of 10 mg.L^{-1}. The first step consists in the adsorption of the pollutant on the surface of the block for 30 min in the dark. Then a UV lamp is used to irradiate the surface of the block containing the photo-catalyst and the concentration is measured at the outlet of the reactor every 2 min. The concentration is determined using a Thermo Scientific Evolution 300 UV-Visible spectrophotometer.Finally, the degradation efficiency (X) of the nanoparticles was estimated by the following equation (2):

$$X = \frac{C_0 - C_f}{C_0} \quad (2)$$

Where C_0 and C_f are the initial and the final concentration of CV.

The experimental device used is represented by the figure2.

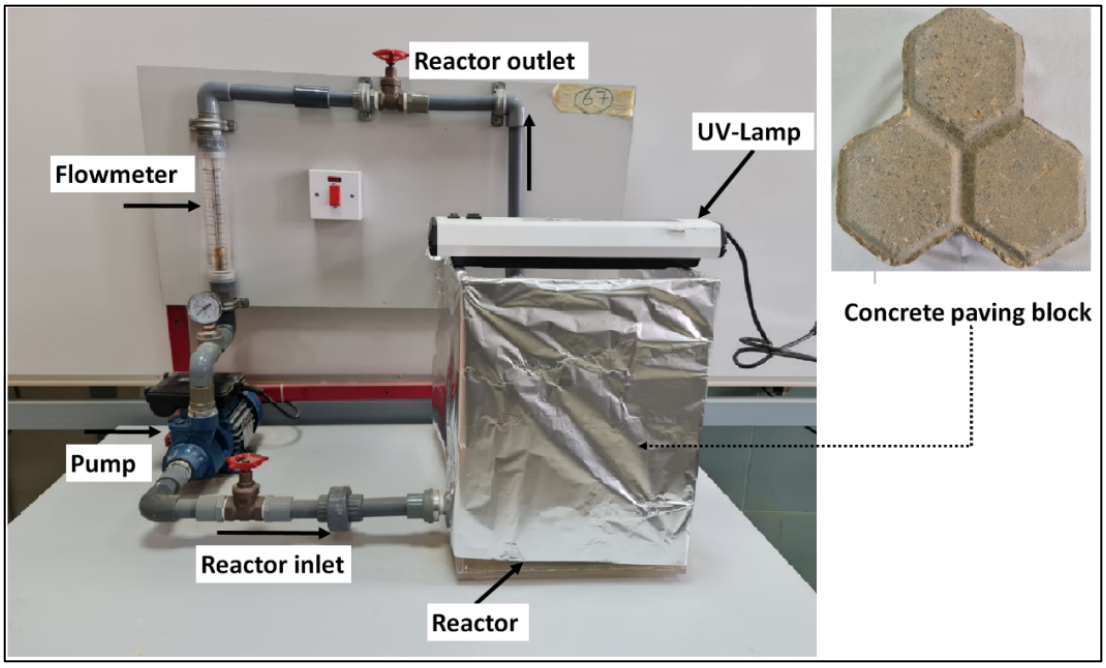

Figure 2: Experimental device of photo-catalytic degradation of (CV) on the surface of the concrete paving block

.

3. RESULTS AND DISCUSSION

3.1 Results of experimental design

The experimental methodology proposed later (table 2) was applied. The nanoparticle synthesis experiments were performed in the order specified by RunOrder (Run order). This order allow to conduct the experiment in random sequence and so to reduce the potential for bias.

For each synthesis experiment, the average particle diameter is estimated from the characterization by X-ray diffraction (XRD) and Scherer's equation (1) as mentioned in section 2.2. By way of illustration, X-ray diffraction (XRD) characterization of the nanoparticles synthesized

in the 7th experiment is represented by the figure 3.

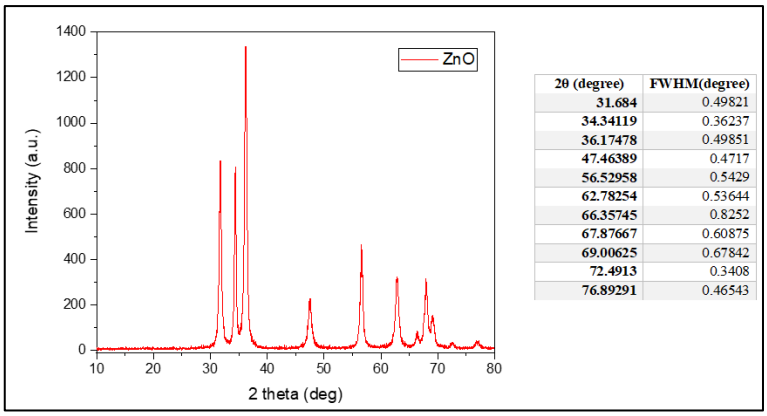

2θ (degree)	FWHM(degree)
31.684	0.49821
34.34119	0.36237
36.17478	0.49851
47.46389	0.4717
56.52958	0.5429
62.78254	0.53644
66.35745	0.8252
67.87667	0.60875
69.00625	0.67842
72.4913	0.3408
76.89291	0.46543

Figure 3: X-ray diffraction (XRD) characterization of ZnO nanoparticles in the 7th experience.

X-ray diffraction (XRD) characterization of ZnO allow to deduce the values of FWHM and then to calculate the average diameter of ZnO particles. It should be noted that the excessive reduction in the size of the particles can lead to the dissolution of the nanoparticles in the synthesis solution and complicates the solid-liquid separation.The average value of the diameter of the nanoparticles, in 7th experience, is equal to 18 nm. The same experimental protocol was applied to the other conditions as shown in Table 3.

Table 3: Results of ZnO nanoparticles diameter.

StdOrder	RunOrder	[Zn-(CH3COO)2,2H2O] (mmol/L)	Temperature (°C)	Stirring time (hr)	dp (nm)
13	**1**	**0.25**	**65**	**3.5**	**16**
7	**2**	**0.1**	**65**	**5**	**16.9**
11	**3**	**0.25**	**50**	**5**	**17**
9	**4**	**0.25**	**50**	**2**	**18**
6	**5**	**0.4**	**65**	**2**	**17.5**
8	**6**	**0.4**	**65**	**5**	**15.5**
2	**7**	**0.4**	**50**	**3.5**	**18**
5	**8**	**0.1**	**65**	**2**	**18**
10	**9**	**0.25**	**80**	**2**	**16.4**
1	**10**	**0.1**	**50**	**3.5**	**19**
15	**11**	**0.25**	**65**	**3.5**	**16**
12	**12**	**0.25**	**80**	**5**	**14.2**
3	**13**	**0.1**	**80**	**3.5**	**16.8**
4	**14**	**0.4**	**80**	**3.5**	**15.2**

14	**15**	**0.25**	**65**	**3.5**	**16**

A comparison of the term's p-value to the significance level can show whether there is a statistically significant relationship between the response and each factor in the model. The null hypothesis is that there is no association between the term and the response because the term's coefficient is equal to zero. The significance value (alpha) in this study is set at 0.05. The results of the experimental design regression and Pareto chart are shown in figure 4.

Term	Coef	SE Coef	T-Value	P-Value	VIF
Constant	16.0000	0.0847	189.00	0.000	
[Zn-(CH3COO)2,2H2O]	-0.5625	0.0518	-10.85	0.000	1.00
Temperature	-1.1750	0.0518	-22.67	0.000	1.00
Stirring time	-0.7875	0.0518	-15.19	0.000	1.00
[Zn-(CH3COO)2,2H2O]*[Zn-(CH3COO)2,2H2O]	0.9125	0.0763	11.96	0.000	1.01
Temperature*Temperature	0.3375	0.0763	4.42	0.007	1.01
Stirring time*Stirring time	0.0625	0.0763	0.82	0.450	1.01
[Zn-(CH3COO)2,2H2O]*Temperature	-0.1500	0.0733	-2.05	0.096	1.00
[Zn-(CH3COO)2,2H2O]*Stirring time	-0.2250	0.0733	-3.07	0.028	1.00
Temperature*Stirring time	-0.3000	0.0733	-4.09	0.009	1.00

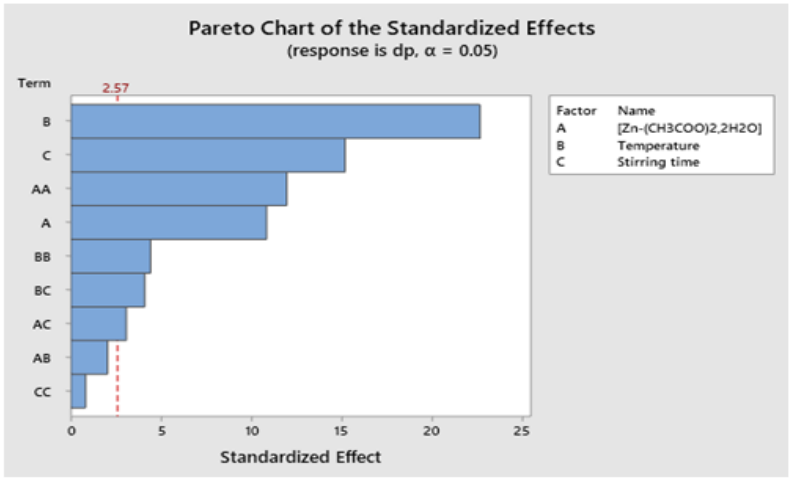

Figure 4: Experimental design regression and Pareto chart.

The Pareto chart of the standardized effects shows that all study factors (temperature, stirring time, and zinc acetate concentration) are significant. Moreover temperature-stirring time and concentration-stirring time interactions are also significant as factors influencing nanoparticle size.

The temperature is the most significant factor on the size of the synthesized particles. Indeed, the increase in temperature promotes the solubility of the precursor (zinc acetate) and accelerates the appearance of nanoparticles. Other research works have mentioned that the addition of NaOH also promotes the dissolution of the initially poorly soluble zinc acetate in the water-ethanol mixture.

For a fixed added quantity of NaoH, temperature is the most significant factor and therefore controls the process of nanoparticle synthesis.

However, it should be noted that Pareto chart makes it possible to judge the significance of the studied factors without showing if the variation of each factor will be beneficial to the minimization of the sizes of synthesized nanoparticles. For this,

a separate analysis of the evolution of the response (size of the particles) according to each factor was carried out. The results are represented by the figure 5.

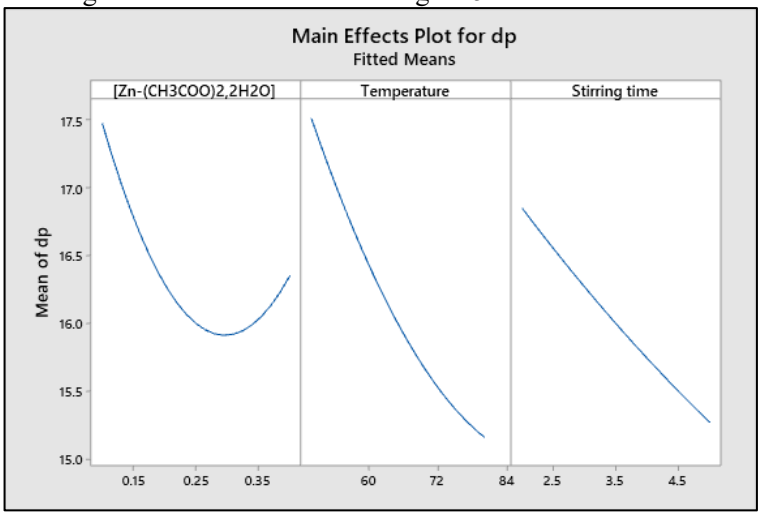

Figure 5: Main effects plots on the nanoparticles size.

Figure 5 shows that increasing the concentration of zinc acetate promotes a reduction in particle size until a limit value of 0.3 mmol/L is reached, which corresponds to a particle size equal to 15.9 nm. Beyond this concentration, the nanoparticle size begins to increase. Consequently, the concentration of zinc acetate is not beneficial in reducing the size of nanoparticles for a value greater than 0.3 mmol/L. The increase in temperature and stirring time promotes the reduction in particle size throughout the experimental variation range. They follow a linear variation trend.

On the other hand, the analysis of the interactions represented by figure 6, makes it possible to understand the impact of the simultaneous variation of the factors. To analyze the effects of interactions the following points have to be considered.

- The parallel lines mean the absence of interaction. The farther the lines are from being parallel, the stronger the interactions.
- As an example, the intersection between column 1 and row 2 indicates the interaction between [Zn-($CH_3COO)_2$, $2H_2O$] and temperature ([Zn-($CH_3COO)_2$,$2H_2O$]*Temperature).

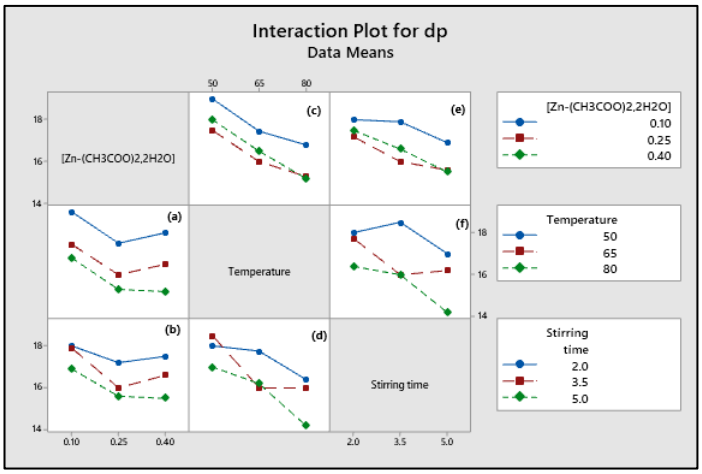

Figure 6: Interaction effects plots on the nanoparticles size.

Figure 6.a and 6.c show the presence of a weak [Zn-$(CH_3COO)_2$,$2H_2O$]*Temperature interaction. This interpretation is consistent with the Pareto chart. Based on the variation of the particle size as a function of the concentration of zinc acetate for different temperatures, we can deduce that the increase in temperature favors the reduction in the size of the particles without however interacting clearly with the Zinc acetate concentration. Similarly, the interaction $(CH_3COO)_2$,$2H_2O$]*stirring time (figures 6.b and 6.e) is weak but more important than the previous interaction. Indeed Pareto chart shows that this interaction is slightly higher than the starting point of significance.

On the other hand, we notice a strong interaction between the temperature and the stirring time represented by figure 6.d and 6.f. the particle size decreases with increasing temperature and stirring speed of 2 and 5h. However, it is noted that the particle size is kept constant in the temperature range between 65 and 80 and for a stirring speed of 3.5h. In this temperature range the effects are compensated.

To better represent the impact of the interactions on the final size of the nanoparticles, the analysis of the contours of the factors is represented by figure 7.

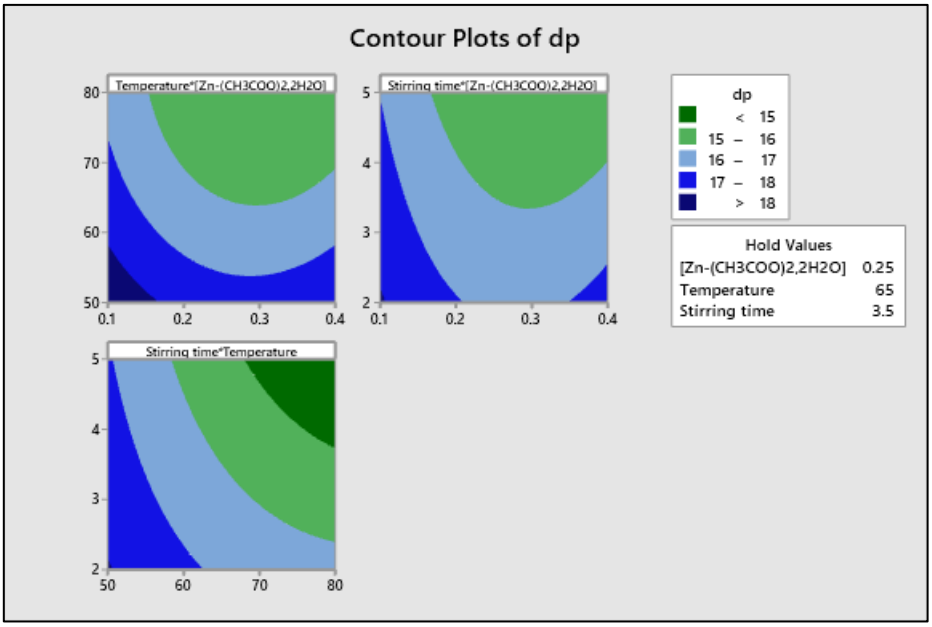

Figure 7: Contour plots of interaction effects on the nanoparticles size.

Figure 7 shows the ranges of concentration, temperature and agitation time allowing to minimize the size of the particles. It is noted that green light zone (15nm<dp<16nm) corresponds to the most favorable zone for minimizing the size of the particles. For cost and experiment time, an experimental point on the border of this area may be chosen. The same observation was concluded for the variation of the stirring time as a function of the concentration.

On the other hand, the areas in blue are experimental conditions to be avoided. For the variation of stirring time as a function of temperature, a new dark green zone appears and gives a particle size of less than 15 nm for large values of temperature and stirring time.

Finally, an optimization of the operating conditions aimed to minimizing the size of the nanoparticles was performed. The optimization results are grouped in the table 4.

Table 4: Optimization results.

Solution	[Zn-(CH3COO)2,2H2O]	Temperature	Stirring time	dp Fit
1	0.327273	80	5	13.8967

The particle size fuction of (temperature (T), stirring time (S.t), and zinc acetate concentration (Z.A)) is given by the regression model equation 3.

$$dp = 10.56 + 47.78\,[Z.A] + 0.15\,T + 2.55S.t - 0.72\,[Z.A] * T - 8.89\,[Z.A] * S.t - 0.04\,T * S.t + 0.11\,[Z.A] * T * S.t \quad (3)$$

The results of the prediction of the minimum particle size value using the regression model (equation 3) is illustrated in Table 5.

Table 5: Confidence and prediction intervals of the optimum result.

Response	Fit	SE Fit	95% CI	95% PI
dp	13.897	0.137	(13.545, 14.248)	(13.381, 14.412)

For the optimal particle size value (13.897nm), the standard error of the fit (SE) is very low (0.137). Consequently, the regression model used is reliable for the prediction of the particle size as a function of the operating conditions. On the other hand, with a confidence level (CL) of 95%, the confidence interval contains the mean of the population of the operating conditions considered. Likewise, the prediction interval indicates that with a 95% of chance one response will be contained in the interval of the chosen operating conditions (variables)(Greenland et al., 2016). For the two confidence indicators, the intervals are small and therefore the prediction is reliable.

3.2 Photo-catalytic tests of concrete paving blocks

The synthesized nanoparticles are placed on the surface of the concrete paving block. Five deposition steps are carried out by drying the blocks each time at 60°C for 2 hours. Then a photo-catalytic test is carried out to evaluate the self-cleaning efficiency of concrete paving block using a model organic pollutant (Crystal viloet). The experimental photo-catalytic protocol is described in section 2.3. The degradation results of the pollutant model (CV) are carried out for different sizes of synthesized particles (14.2 nm, 16.8 nm, 19 nm) and an average particle size of commercial ZnO (50 nm). The maximum conversion rate (X) reached for each chosen particle size is shown in Figure 8.

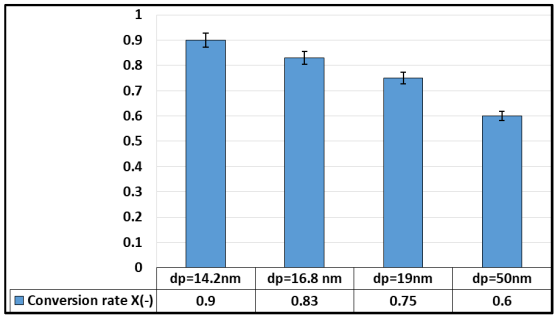

Figure 8: Maximum conversion rate (X) reached for each chosen particle size.

Figure 8 shows that the maximum conversion rate reached increases with the reduction in the size of the photo-catalyst particles. Indeed, the reduction in the size of the particles increases the specific surface of the concrete paving block: If we compare the shape of the photo-catalyst (ZnO) to a spherical particle, the relation of the specific surface (S_{sp}) according to the size of the particle (r) is given by the equation 4 (Hariharan, 2006):

$$S_{sp} = \frac{3}{\rho r} \quad (4)$$

In the other hand, the effect of particle size on the UV radiation penetration of photo-catalyst is a significant factor to consider. Studies have found that smaller particles are more effective, allowing more radiation penetration and therefore allowing for better catalytic performance (Chen et al., 2018; Corma, Martınez, & Martınez-Soria, 2001; Lv et al., 2023; W. Wang et al., 2023). This is due to the larger surface area in contact with the UV radiation, which increases the reaction rate, resulting in improved photo-catalytic performance. The particle size of a photo-catalyst is therefore an important factor in optimizing UV radiation penetration and maximizing its catalytic efficiency(Roy, Mondal, & Mitra, 2023; Y. Wang et al., 2022).

In addition, the rate of photo-catalytic degradation is analyzed by the temporal evolution of the conversion rate of (CV) as shown in Figure 9.

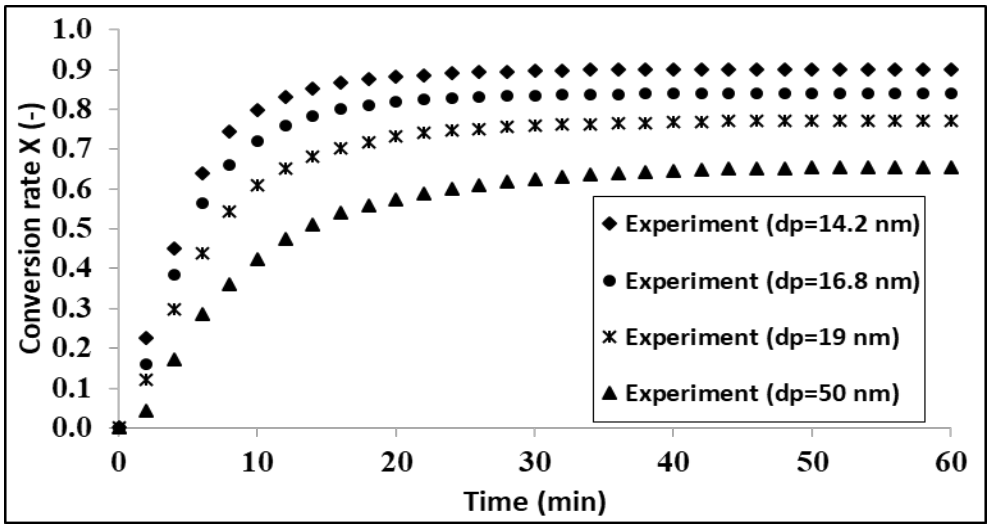

Figure 9: Temporal evolution of the conversion rate of (CV)

Figure 9 shows that in addition to its effect on overall conversion rate, particle size also affects the reaction rate. Indeed, the temporal evolution of the rate of conversion rate for the particles size of 50 nm shows that the maximum conversion rate is reached after 40 min. The smaller the size, the greater the reaction rate becomes. The conversion times of (CV) are 32 min, 26 min and 23 min for the particle sizes 19nm, 16.8nm and 14.2nm respectively. The results show that decreasing the particle size from 50 nm to 14.2 nm improves the maximum conversion rate by 33% and an acceleration of the reaction rate by 28%.

Therefore, decreasing the particle size is an effective way to enhance the conversion rate as well as the rate of reaction, thus allowing for shorter reaction times with higher yields. This is because decreasing the particle size increases the surface area of the reactants, resulting in more collisions and better mass transfer between phases. This can be especially beneficial when dealing with low solubility reactants since smaller

particles will have a greater chance of coming into contact with each other.
The second approach in this section concerns a numerical simulation by COMSOL Multiphysics©. This simulation is based on the finite element method allowing a numerical resolution of the transport and diffusion equations of the pollutant (CV) (equation 5), and of the catalytic degradation reaction at the surface of concrete paving blocks.

$$\frac{\partial C}{\partial t} + \nabla . J + u . \nabla C = R \quad and \quad J = -D\nabla C \qquad (5)$$

With:
C the pollutant concentration (CV) at the concrete paving block surface,
U: the flow velocity of the pollutant on the concrete paving block surface,
A: the speed of the reaction on the surface of concrete paving block,
D: the coefficient of the pollutant diffusion (CV).
To solve the differential equation (Eq5) by finite element method, a temporal and spatial discretization was performed. The geometry was designed with the real dimensions of the concrete paving block (figure 10.a). Then a parametric study of the mesh of the geometry was developed and allowed to choose the shape and the size of elements represented by figure 10.b. The numerical resolution with a total number of elements of 306175, ensured the simulation with reasonable computation time (30min) and accuracy.

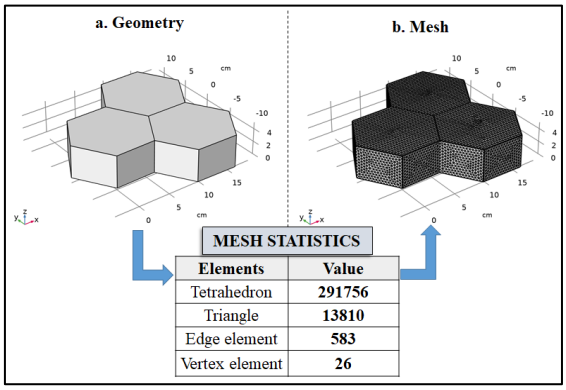

Figure 10: Geometry and mesh of simulated concrete paving block.

The concentration profile at the surface of the concrete paving block is estimated, by simulation, as a function of time for the minimum particle size (14.2 nm) as represented by figure 11.

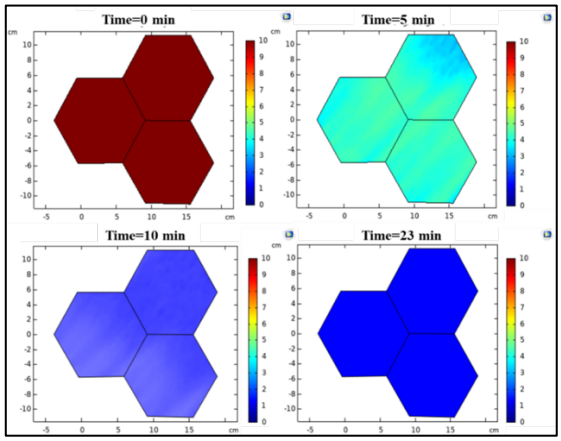

Figure 11: Concentration profiles at the surface of the concrete paving block.

Figure 11 shows that the average concentration at the surface for t=0min is equal to 10mg/L. Then the concentration decreases gradually to reach the values of 4.30mg/L, 1.80 mg/L, and 0.85 mg/L for the respective times 5min, 10min and 23min. The maximum conversion rate achieved is 91.5%.

The uniformity of the concentration at the surface can be explained by the step that controls the photo-catalytic degradation process: the reaction rate is faster than the transport of the pollutant on the catalyst and therefore the pollutant degrades rapidly compared to its residence time crossing the surface.

Finally, to validate the numerical model simulating the self-cleaning concrete paving block, a comparison of the experimental and modeled reaction rates was established as represented by figure 12.

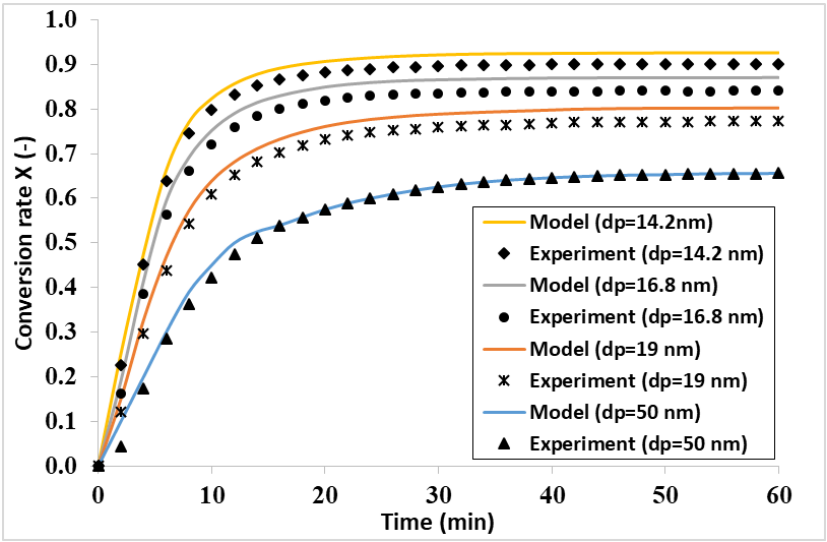

Figure 12: Concentration profiles at the surface of the concrete paving block.

For the diameter of 50 nm, the simulation results fit the experiments correctly. For smaller particle sizes, simulation results show slightly higher conversion rates than experiments (2 to 3%). This difference can be explained by the perfect homogeneity of the dispersion of the photo-catalyst, on the concrete paving block, in simulations against slight defiance in the real

dispersion of the photo-catalyst in the experiments.

4. CONCLUSION

The application of photo-catalytic self-cleaning concrete to remove organic impurities from water was the main concern of this work. Photo-catalyst nanoparticles was used in order to stabilize the catalyst and avoid electron-hole recombination events in the semiconductor. The produced photo-catalyst is then applied to the surface of the blocks of concrete blocks. The experimental conduct of nanoparticle synthesis was optimized using a response surface methodology (RSM). The effect of stirring speed, the temperature and the concentration of zinc acetate on the nanoparticles diameter were studied. A Box-Behnken (BB) design with three factors and three center points was used. For each synthesis experiment, the average of particles diameter is estimated from the (XRD) characterization and Scherer's equation. All research parameters (temperature, stirring duration, and zinc acetate concentration) are significant, as shown by the Pareto chart of the standardized effects. Moreover, relationships between temperature and stirring time and concentration and stirring time are significant factors. The size of the synthesized particles is most significantly influenced by temperature. In fact, when the temperature increases, the precursor (zinc acetate) becomes more soluble and the emergence of nanoparticles occurs faster. It should be highlighted that the most effective zone for reducing particle size corresponds to the green light zone (15nm-dp-16nm). The variation in stirring time as a function of concentration was found to behave similarly.

For the optimal particle size value (13.897nm), the standard error of the fit (SE) is very low (0.137). Consequently, the regression model used is reliable for the prediction of the particle size as a function of the operating conditions.

The degradation results of the pollutant model (CV) are carried out for different sizes of synthesized particles (14.2 nm, 16.8 nm, 19 nm) and an average particle size of commercial ZnO (50 nm). The temporal evolution of the conversion rate for the particles size of 50 nm shows that the maximum conversion rate is reached after 40 min. The smaller the size, the greater the reaction rate becomes. The results show that decreasing the particle size from 50 nm to 14.2 nm improves the maximum conversion rate by 33% and an acceleration of the reaction rate by 28%. Therefore, decreasing the particle size is an effective way to enhance the conversion rate as well as the rate of reaction, thus allowing for shorter reaction times with higher yields.

The concentration profile at the surface of the concrete paving block is estimated, by simulation, as a function of time for the minimum particle size (14.2 nm). The average concentration at the surface for t=0min is equal to 10mg/L. Then the concentration decreases gradually to reach the values of 4.30mg/L, 1.80 mg/L, and 0.85 mg/L for the respective times 5min, 10min and 23min. The maximum conversion rate achieved is 91.5%. The uniformity of the concentration at the surface of concrete paving block can be explained by the step that controls the photo-catalytic degradation process: the reaction rate is faster than the transport of the pollutant on the catalyst and therefore the pollutant degrades rapidly compared to its residence time crossing the surface.

Finally, to validate the numerical model simulating the self-cleaning concrete paving block, a comparison of the experimental and modeled reaction rates was established. For the diameter of 50 nm, the simulation results fit the experiments correctly. For smaller particle sizes, simulation results show slightly higher conversion rates than experiments (2 to 3%). This difference can be explained by the perfect homogeneity of the dispersion of the photo-catalyst, on the concrete paving block, in simulations against slight defiance in the real dispersion of the photo-catalyst in the experiments.

References

Abukhadra, M. R., AlHammadi, A. A., Khim, J. S., Ajarem, J. S., & Allam, A. A. (2022). Enhanced decontamination of levofloxacin residuals from water using recycled glass based a green zinc oxide/mesoporous silica nanocomposite; adsorption and advanced oxidation studies. Journal of Cleaner Production, 356, 131836.

Ahamed, I., Ahamed, M., Kumar, K. S., & Sivaranjani, A. (2022). Comparative energy bandgap analysis of zinc and tin based chalcogenide quantum dots. Revista Mexicana de Física, 68(4 Jul-Aug), 041601 041601–041608-041601 041601–041608.

Alrwis, K. N., Ghanem, A. M., Alnashwan, O. S., Al Duwais, A. A. M., Alaagib, S. A. B., & Aldawdahi, N. M. (2021). Measuring the impact of water scarcity on agricultural economic development in saudi arabia. Saudi Journal of Biological Sciences, 28(1), 191-195.

Awadalla, A., Zain, M. M., Kadhum, A. A. H., & Abdalla, Z. (2011). Titanium dioxide as photocatalyses to create self-cleaning concrete and improve indoor air quality. International Journal of the Physical Sciences, 6(29), 6767-6774.

Baig, M. B., Alotibi, Y., Straquadine, G. S., & Alataway, A. (2020). Water resources in the kingdom of saudi arabia: Challenges and strategies for improvement. Water Policies in MENA Countries, 135-160.

Caudillo-Flores, U., Muñoz-Batista, M. J., Fernández-García, M., & Kubacka, A. (2022). Recent progress in the quantitative assessment and interpretation of photoactivity. Catalysis Reviews, 1-55.

Chen, X., Yu, E., Cai, S., Jia, H., Chen, J., & Liang, P. (2018). In situ pyrolysis of ce-mof to prepare ceo2 catalyst with obviously improved catalytic performance for toluene combustion. Chemical Engineering Journal, 344, 469-479.

Corma, A., Martınez, A., & Martınez-Soria, V. (2001). Catalytic performance of the new delaminated itq-2 zeolite for mild hydrocracking and aromatic hydrogenation processes. Journal of Catalysis, 200(2), 259-269.

Deng, Y. (2021). Pollution in rainwater harvesting: A challenge for sustainability and resilience of urban agriculture. Journal of Hazardous Materials Letters, 2, 100037.

El-Morsy, M., Awwad, N. S., Ali, H. E., & Menazea, A. (2022). Optical, thermal and dielectric properties of copper oxide (cuo)/chitosan (cs)/polyethylene oxide (peo) blends. Journal of Polymer Research, 29(5), 177.

Gaur, N., Dutta, D., Singh, A., Dubey, R., & Kamboj, D. V. (2022). Recent advances in the elimination of persistent organic pollutants by photocatalysis. Frontiers in Environmental Science, 10, 2076.

Greenland, S., Senn, S. J., Rothman, K. J., Carlin, J. B., Poole, C., Goodman, S. N., & Altman, D. G. (2016). Statistical tests, p values, confidence intervals, and power: A guide to misinterpretations. European journal of epidemiology, 31, 337-350.

Gul, B., Khan, M. S., Khan, G., Ahmad, H., Thounthong, P., Khattak, S. A., . . . Khan, T. (2022). First-principles calculations to investigate the optoelectronic, and thermoelectric nature of zinc based group ii-vi direct band semiconductors. Optik, 271, 170143.

Hariharan, C. (2006). Photocatalytic degradation of organic contaminants in water by zno nanoparticles: Revisited. Applied Catalysis A: General, 304, 55-61.

Hassan, G., Yilbas, B. S., Al-Sharafi, A., Sahin, A. Z., & Al-Qahtani, H. (2020). Solar energy harvesting and self-cleaning of surfaces by an impacting water droplet. International Journal of Energy Research, 44(1), 388-401.

Hossain, M. S., Jahan, S. A., & Ahmed, S. (2023). Crystallographic characterization of bio-waste material originated caco3, green-synthesized cao and ca (oh) 2. Results in Chemistry, 100822.

Iqbal, A., Yusaf, A., Usman, M., Hussain Bokhari, T., & Mansha, A. (2023). Insight into the degradation of different classes of dyes by advanced oxidation processes; a detailed review. International Journal of Environmental Analytical Chemistry, 1-35.

Kalyani, N. T., & Dhoble, S. J. (2023). Introduction to nano materials. In Quantum dots (pp. 3-40): Elsevier.

Karpińska, J., & Kotowska, U. (2019). Removal of organic pollution in the water environment. In (Vol. 11, pp. 2017): MDPI.

Lee, S.-Y., & Park, S.-J. (2013). Tio2 photocatalyst for water treatment applications. Journal of industrial and engineering chemistry, 19(6), 1761-1769.

Liu, Z., Liu, X., Yu, J., Copeland, L., & Wang, S. (2023). Novel approach for quantitative characterization of short-range molecular order in gelatinized starch by x-ray diffraction. Biomacromolecules.

Lv, C., Bai, X., Ning, S., Song, C., Guan, Q., Liu, B., . . . Ye, J. (2023). Nanostructured materials for photothermal carbon dioxide hydrogenation: Regulating solar utilization and catalytic performance. ACS nano.

Lvov, K., Potemkin, F., & Stremoukhov, S. Y. (2023). Extension of the multiple rate equation model for conduction band dynamics under near-and mid-ir femtosecond excitation of dielectrics and semiconductors. Materials Today Communications, 105594.

Mishra, R., Pandey, S., & Fosso-Kankeu, E. (2023). Role of heterogeneous catalysts for advanced oxidation process in wastewater treatment. Photoreactors in Advanced Oxidation Process: The Future of Wastewater Treatment, 37.

Modi, S., Yadav, V. K., Gacem, A., Ali, I. H., Dave, D., Khan, S. H., . . . Son, C. T. (2022). Recent and emerging trends in remediation of methylene blue dye from wastewater by using zinc oxide nanoparticles. Water, 14(11), 1749.

Napoli, F. S. R., Uriarte, D., Garrido, M., Domini, C., & Acebal, C. (2022). Nanophotocatalysis for degradation of organic contaminants. In Handbook of green and sustainable nanotechnology:

Fundamentals, developments and applications (pp. 1-43): Springer.

Ningthoujam, R., Singh, Y. D., Babu, P. J., Tirkey, A., Pardhan, S., & Sarma, M. (2022). Nanocatalyst in remediating environmental pollutants. Chemical Physics Impact, 100064.

Paolini, R., Borroni, D., Pedeferri, M., & Diamanti, M. V. (2018). Self-cleaning building materials: The multifaceted effects of titanium dioxide. Construction and Building Materials, 182, 126-133.

Pattnaik, A., Sahu, J., Poonia, A. K., & Ghosh, P. (2023). Current perspective of nano-engineered metal oxide based photocatalysts in advanced oxidation processes for degradation of organic pollutants in wastewater. Chemical Engineering Research and Design.

Qualharini, E. L., Stolz, C. M., Martini, M., Polesello, E., & da Silva, C. R. (2023). Self-cleaning mortar façades with addition of anatase and rutile titanium dioxide for cool façades. Energies, 16(4), 1874.

Roy, T. K., Mondal, N. K., & Mitra, P. (2023). Efficacy of mn-doped zno towards removal of congo red dye under uv exposure: Isotherm, kinetics, thermodynamics and optimization study. Pollution, 9(2), 513-530.

Singh, S., Yadav, R., Kathi, S., & Singh, A. N. (2022). Treatment of harvested rainwater and reuse: Practices, prospects, and challenges. Cost Effective Technologies for Solid Waste and Wastewater Treatment, 161-178.

Singh, V., Gautam, S., Kaur, S., Kajal, N., Kaur, M., & Gupta, R. (2022). Highly functionalized photo-activated metal–organic frameworks for dye degradation: Recent advancements. Materials Today Communications, 105180.

Song, C.-G., Liu, Y.-Q., Ding, G., Yang, J., Wang, C.-Y., Wu, J.-R., . . . Qin, J.-C. (2022). Synergistic adsorption–photocatalysis based on magnetic metal–organic framework nanoplatforms for organic pollutant removal. ACS Applied Nano Materials.

Torres-Torres, C., & García-Beltrán, G. (2022). Study on second-and third-order nonlinear optical properties in semiconductor nanoparticles and quantum dots. In Optical nonlinearities in nanostructured systems (pp. 109-123): Springer.

Van Thuan, D., Nguyen, T. L., Thi, H. H. P., Thanh, N. T., Ghotekar, S., Sharma, A. K., . . . Cam, D. P. (2022). Development of indium vanadate and silver deposited on graphitic carbon nitride ternary heterojunction for advanced photocatalytic degradation of residual antibiotics in aqueous environment. Optical Materials, 123, 111885.

Wang, W., Duong-Viet, C., Truong-Phuoc, L., Truong-Huu, T., Nguyen, H. M., Nguyen-Dinh, L., . . . Pham-Huu, C. (2023). Improving catalytic performance via induction heating: Selective oxidation of h 2 s on a nitrogen-doped carbon catalyst as a model reaction. New Journal of Chemistry, 47(3), 1105-1116.

Wang, Y., Zhang, H., Liu, Y., Younis, M. H., Cai, W., & Bu, W. (2022). Catalytic radiosensitization: Insights from materials physicochemistry. Materials Today.

Wouters, R. D., Muraro, P. C. L., Druzian, D. M., Viana, A. R., de Oliveira Pinto, E., da Silva, J. K. L., . . . Pavoski, G. (2023). Zinc oxide nanoparticles: Biosynthesis, characterization, biological activity and photocatalytic degradation for tartrazine yellow dye. Journal of Molecular Liquids, 371, 121090.

Wu, Y., Du, J., Liu, G., Ma, D., Jia, F., Klemeš, J. J., & Wang, J. (2021). A review of self-cleaning technology to reduce dust and ice accumulation in photovoltaic power generation using superhydrophobic coating. Renewable Energy.

Xia, Y., Zhu, N., Zhao, Y., Zhu, J., Chen, H., Xu, L., & Yao, L. (2023). Construction of durable self-cleaning pdms film on polyester fabric surface. Materials, 16(1), 52.

Yao, Z., Wang, M., Jia, R., Zhao, Q., Liu, L., & Sun, S. (2023). Comparison of uv-based advanced oxidation processes for the removal of different fractions of nom from drinking water. Journal of Environmental Sciences, 126, 387-395.